Calculated Phase Diagrams, Iron Tolerance Limits, and Corrosion of Mg-Al Alloys

Ming Liu, Peter J. Uggowitzer, Patrik Schmutz, and Andrej Atrens

The factors determining corrosion are reviewed in this paper, with an emphasis on iron tolerance limit and the production of high-purity castings. To understand the iron impurity tolerance limit, magnesium phase diagrams were calculated using the Pandat *software package. Calculated phase diagrams can explain the iron tolerance limit and the production of high-purity castings by means of control of melt conditions; this is significant for the production of quality castings from recycled magnesium. Based on the new insight, the influence of the microstructure on corrosion of magnesium alloys is reviewed.*

INTRODUCTION

Magnesium alloys are used in transportation applications due to their low density and adequate strength/weight ratio. A limitation to their service use is corrosion[1–5] and hence there is much effort to understand their corrosion behavior.[6–60] An important aspect of the corrosion of magnesium alloys is the high sensitivity to the impurity elements Fe, Ni, Cu, and Co. The corrosion of commercial alloys is dominated by the iron content above the iron tolerance limit, and high corrosion rates are expected. For iron contents below the tolerance limits, other factors can influence the corrosion behavior, such as chemical composition and microstructure. The calculated magnesium phase diagrams indicate that the iron impurity tolerance limit is caused by the precipitation of a distinct, iron-rich phase.

Corrosion of Magnesium Alloys

Stress corrosion cracking (SCC) occurs in frequently encountered environments[61–70] including distilled water,[61–66] indicating that water itself is the key environmental factor causing SCC in aqueous solutions. The key points of the corrosion mechanism for magnesium alloys[1–3] are as follows. A partially protective oxide/hydroxide film covers the surface and corrosion occurs at the breaks in this film. The cathodic reaction is hydrogen production. The surface film on magnesium is not particularly protective; the corrosion rate is typically more than 1 mm/y in common environments like 3% NaCl solution. No alloying element has been discovered that produces a solid-solution magnesium alloy with a corrosion rate less than that of pure magnesium in 3% NaCl solution. Consequently, it is useful to include pure magnesium as a standard in any comparative study of corrosion performance of magnesium alloys;[2,21,35] commercial purity magnesium can have a corrosion rate more than 50 times that of pure magnesium.[2,17]

Corrosion of common magnesium alloys typically involves micro-galvanic acceleration[2,17,21,34–36] of the corrosion of the α-Mg matrix by the second phase(s). The corrosion rate of a two-phase magnesium alloy can, however, be lower than that of pure magnesium if the second phase is finely divided, essentially continuous, and the second phase itself has a lower corrosion rate than that of pure magnesium. Then, the second phase can act as a corrosion barrier. The corrosion form of magnesium is typically designated as localized corrosion[1,2,36,38] to distinguish it from the auto-catalytic pitting in stainless steels.

Corrosion of magnesium has a number of seemingly strange phenomena. The best known is the negative difference effect.[1–3,32,33] This effect means that the amount of hydrogen liberated

How would *you…*

…describe the overall significance of this paper?

Magnesium alloys are used in transportation due to their low density and adequate strength/weight ratio. A limitation to their service use, however, is corrosion. An important aspect of the corrosion of magnesium alloys is the high sensitivity to the impurity elements Fe, Ni, Cu, and Co. The corrosion rate is low up to a tolerance limit and substantially higher above the tolerance limit. The factors determining corrosion are reviewed, with an emphasis on the iron tolerance limit and the production of high-purity castings.

…describe this work to a materials science and engineering professional with no experience in your technical specialty?

The iron tolerance limit for magnesium is explained by using the calculated phase diagram. Above the tolerance limit, a separate iron-rich phase forms as a magnesium alloy casting solidifies. This phase is an efficient cathode and accelerates the corrosion of the alloy by micro-galvanic coupling to accelerate the corrosion of the magnesium matrix. The phase diagram predicts that the iron tolerance limit is 180 ppm in good agreement with prior experiment.

…describe this work to a layperson?

Corrosion of magnesium alloys limits their use in applications such as cars, where the magnesium alloys could lead to lighter, more-fuel-efficient, more-environmentally friendly cars. A practical issue for magnesium alloys is that a small content of iron (170 ppm) leads to high corrosion rates. This work explains that above 180 ppm there is a change of the magnesium alloy that causes the high corrosion rates, and how good low-iron castings can be made from poor high-iron feedstock.

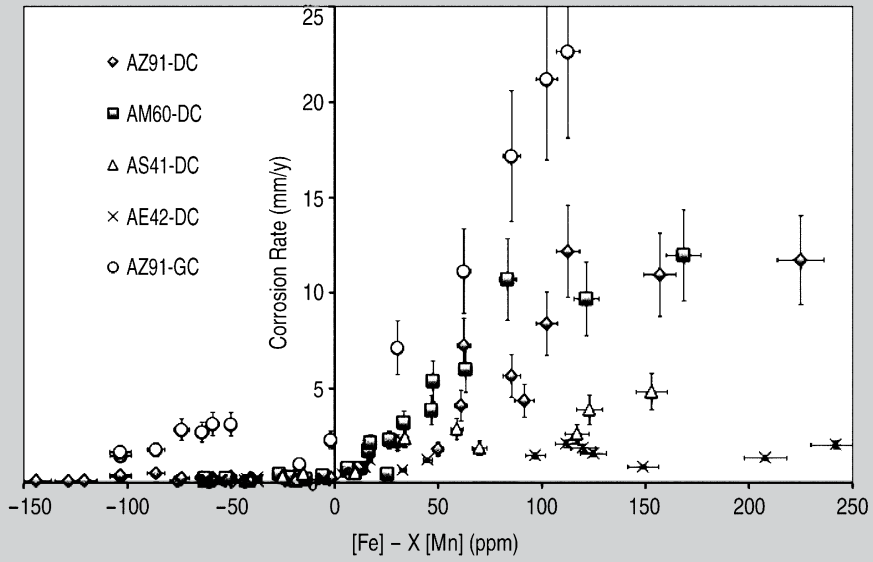

Figure 1. For the magnesium alloys AZ91, AM60, AS41, and AE42, the salt spray corrosion rate (mm/y) as a function of the alloy iron content ([Fe]) above the tolerance limit (X[Mn]) at the alloy manganese content ([Mn]).

increases with increasing applied anodic current (which decreases the cathodic reaction rate and the amount of associated "cathodic" hydrogen) and the amount of magnesium dissolved is greater than expected from application of the Faraday Law. Another well-known effect is that electrochemical measurements of the corrosion rate, based on the corrosion current at the free corrosion potential, do not agree with direct measurements using weight loss or evaluated from the evolved hydrogen.[2,30,36,40,71]

Influence of Iron on Magnesium Corrosion

The corrosion rate is low up to a tolerance limit; the corrosion rate is substantially higher above the tolerance limit (the factor may be 100×). Typical values of tolerance limits are given in Table I. There are two hypotheses[1,2] for the tolerance limits of Fe, Ni, Cu, and Co: phase precipitation and surface deposition. Both the phase precipitation and surface deposition hypotheses assume that effective hydrogen cathodes are produced above the tolerance limit, and both assume that these cathodes have a composition rich in the impurity element. The essential difference is that the phase precipitation hypothesis relates to the precipitation of a new phase inside the magnesium alloy whereas the surface deposition hypothesis relates to the deposition of cathodes on the magnesium alloy surface. To date there has been no successful resolution regarding which hypothesis is correct.

Some useful insights are gained regarding the mechanism of the iron tolerance limit for the die-cast (DC) and gravity-cast (GC) magnesium alloys AZ91-DC and AZ91-GC,[6] AM60-DC,[12] AS41-DC,[10] and AE42-DC.[13] Figure 1 presents the salt spray corrosion rate (measured over 10 days) as a function of the iron content above the tolerance limit evaluated as "[Fe] – X×[Mn]", where [Fe] is the iron content of the alloy, [Mn] is the manganese content of the alloy, and X×[Mn] is the alloy-dependent iron tolerance limit which depends on the manganese concentration and on the alloy (i.e., the weighting factor X is alloy-dependent, particularly dependent on alloy aluminum content, as shown in Table I). Figure 1 shows that, first, the corrosion rate is low below the tolerance limit and high above the tolerance limit, and second, above the tolerance limit, the corrosion rate increases rapidly in a non-linear fashion, which is dependent on the alloy and casting method.

This behavior is consistent with a second phase above the tolerance limit, with the phase in each case having somewhat different ability to act as a cathode and liberate hydrogen. It is hard to reconcile Figure 1 with the second explanation for the tolerance limit, namely that the probability of producing surface iron cathodes increases with iron content.

High-Purity Castings

That the tolerance level is related to the precipitation of a separate phase is also supported by the controlled casting experiments of J.E. Hillis and coworkers using AZ91,[6] AM60,[12] and AS41.[10] These experiments demonstrated that high-purity alloys could be

Table I. Tolerance Limits for Magnesium Alloys[1]

Alloy	Condition	Fe	Ni (ppm)	Cu (ppm)	Reference
Pure Mg		170 ppm	5	1,000	4
Pure Mg		170 ppm	5	1,300	5
AZ91		20 ppm	12	900	5
AZ91		0.032∗Mn	50	400	4,6
AZ91	HPDC (F)	0.032∗Mn	50	400	7,8
AZ91	LPDC (F)	0.032∗Mn	10	400	7
AZ91	LPDC (T4)	0.035∗Mn	10	100	6,7
AZ91	LPDC (T6)	0.046∗Mn	10	400	7
AZ91B			<100	< 2,500	9
AZ91	Die cast	0.032∗Mn	50	400	10
AZ91	Die cast	50 ppm	50	700	9
AZ91	Die cast	0.032∗Mn	50	700	6
AZ91	Gravity cast	0.032∗Mn	10	400	6
AM60	Die cast	0.021∗Mn	30	10	10–12
AE42	Die cast	0.020∗Mn	40	400	13
AS41	Die cast	0.010∗Mn	40	200	10–13

*HPDC = high-pressure die cast; LPDC = low-pressure die cast

produced from low-purity alloys by control of the casting temperature. For the AZ91 experiments, they used ~40 kg heats of high-purity AZ91-base alloys containing ~9%Al, 0.5%Zn, ~390 ppm Fe, <10 ppm Ni and <100 ppm Cu. The alloy was equilibrated with 0.2%Mn (trial 1), 0.4%Mn (trial 2), or 0.8%Mn (trial 3) at 750ºC; die castings were made at 750ºC and after equilibration for 10–15 min. at three lower nominal temperatures: 725ºC, 690ºC, and 650ºC (in each case they measured the actual temperature of the melt at the time of casting, and these actual temperatures were somewhat different than the nominal temperatures).

Chemical analysis of the die castings revealed the chemical composition of the melt just before casting. Chemical analysis of the die castings of trial 1 indicated a decrease in only the iron content as the melt temperature was decreased from 750ºC to 690ºC, consistent with the precipitation from the melt of an iron-rich phase containing no manganese; each of these die castings had an iron content above the manganese-dependent tolerance limit and had a high corrosion rate in the salt spray test. The trial 1 die-casting at 650ºC had a lower iron composition and a lower manganese composition, indicating the precipitation of both these elements from the melt between 690ºC and 650ºC, which could be by the precipitation of a single Fe_aMn_b compound or by the precipitation of two compounds, one iron-rich, the other manganese rich. The trial 1 650ºC casting had an iron content below the tolerance limit and a low corrosion rate in the salt spray test. The other trials with AZ91,[6] and the subsequent trials with AM60[12] and AS41,[10] revealed similar trends. Table II presents the values of the measured critical melt temperature, T_M, at which castings were produced with measured low corrosion rates and above which there was precipitation of both iron and manganese from the melt.

Table II. Values of the Measured Critical Melt Temperature, T_M, Measured for AZ91[6], AM60[12], and AS41[10]*

Alloy	Al (wt.%)	$[Mn]_{750ºC}$ (wt.%)	T_M (ºC)	T_C (ºC)
AZ91	9	0.2	654	640
AZ91	9	0.4	694	690
AZ91	9	0.8	>750	760
AM60	6	0.2	640	620
AM60	6	0.4	650	670
AM60	6	0.8	720	720
AS41	4	0.2	<660	620
AS41	4	0.4	658	630
AS41	4	0.8	—	685

* T_M is the temperature at which low corrosion rates were measured and above which there was precipitation of both Fe and Mn from the melt. $[Mn]_{750ºC}$ is the Mn concentration in the starting melt at 750ºC; the die castings typically contained a lower Mn concentration. T_C is the temperature at which the calculated Mg-Al-Mn-Fe phase diagrams predict that solidification of a casting would lead to no BCC phase in the casting.

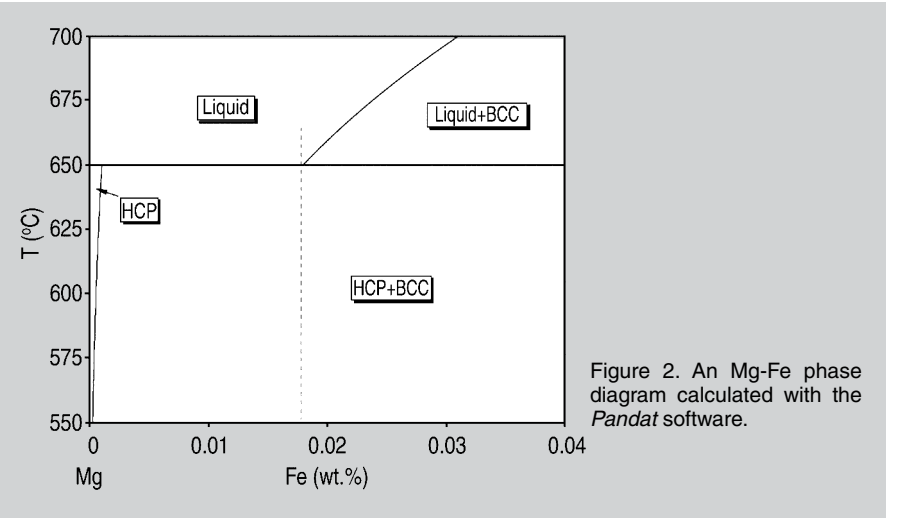

Figure 2. An Mg-Fe phase diagram calculated with the *Pandat* software.

Research Goals

The present study has the following aims: use calculated magnesium phase diagrams to understand the metallurgy of the influence of iron impurities on the corrosion of magnesium alloys, and use calculated magnesium phase diagrams to explain the production of high-purity magnesium castings by controlling melt conditions so that the castings have excellent corrosion properties.

CALCULATED PHASE DIAGRAMS

To understand the iron impurity tolerance limit, magnesium phase diagrams were calculated using the *Pandat* software package (database PanMg7; it comprises 18 components with the following composition limits: 0–10 wt.% for Al, Ca, Li, Mn, Si, and Zn; 0–1 wt.% for Ag, Ce, Gd, Nd, Sc, Sn, Sr, Y, Zr, Fe, and Cu; 346 different phases are considered).[72] The phase diagrams so calculated use the thermodynamic data in the latest *Pandat* magnesium database. The thermodynamic data has not been optimized at all for these calculations. Thus, it is likely that particular numerical values may be somewhat in error, but the trends can be assumed to be valid. Furthermore, the database is not complete; it includes data for iron and copper, but not nickel or cobalt. For the present case, phase diagrams have been calculated to understand the tolerance limit for iron.

Table III. Details of Phases in the Calculated Phase Diagrams

Phase Diagram	Phase	Details
Mg-Fe (Figure 2)	BCC	Essentially pure Fe containing little Mg in solid solution
	HCP	Alpha-Mg containing little Fe in solid solution
Mg-Al-Fe (Figure 3)	BCC	Essentially Fe containing some Al and little Mg in solid solution
Mg-0.4Mn-0.02Fe-Al (Figure 4)	BCC_B2	Fe-Mn-Al phase; basically the same phase as BCC in the Mg-Fe phase diagram, containing some Mn.
	Al_8Mn_5	Al_8Mn_5

*BCC = body-centered cubic; HCP = hexagonal close-packed

Mg-Fe

Figure 2 presents the calculated Mg-Fe phase diagram: a eutectic system with a eutectic temperature of 650ºC, and a maximum solubility of ≈10 ppm iron. Table III presents details of the phases in the calculated phase diagrams.

Cooling of an Mg-Fe alloy containing more than 180 ppm is predicted to cause the solidification, from the melt, of a separate body-centered cubic (BCC) phase. For an iron content of less than 180 ppm the calculated phase diagram predicts that on cooling the liquid magnesium alloy undergoes eutectic solidification at 650ºC to form α-Mg containing about 10 ppm iron in solid solution plus the BCC phase. However, the two-phase region (liquid Mg + α-Mg) is extremely narrow, so that it would be expected that the pre-eutectic and eutectic reaction would be suppressed during normal (non-equilibrium) cooling of a magnesium ingot or casting. Thus a magnesium alloy containing less than 180 ppm iron would solidify to a single α-Mg phase with iron in solid solution in the magnesium lattice. If this is indeed correct, the implication is that there is single-phase magnesium up to a critical iron concentration of 180 ppm and that there would be a separate BCC phase (rich in iron) for a magnesium casting with an iron content greater than 180 ppm.

This value of 180 ppm iron should be compared with the iron tolerance level in pure as-cast magnesium reported to be 170 ppm[1,4,6] or 150 ppm.[7] The calculated phase diagram thus offers an explanation of the iron tolerance limit: It corresponds to the minimum content of iron in a cast magnesium alloy for which a BCC phase solidifies from the melt before final solidification.

The phase diagram allows an estimation of how much second phase forms for a given alloy in equilibrium. For a magnesium alloy containing 280 ppm iron, the fraction of the primary BCC phase, $f_{BCC/casting}$, can be calculated using the lever rule as follows:

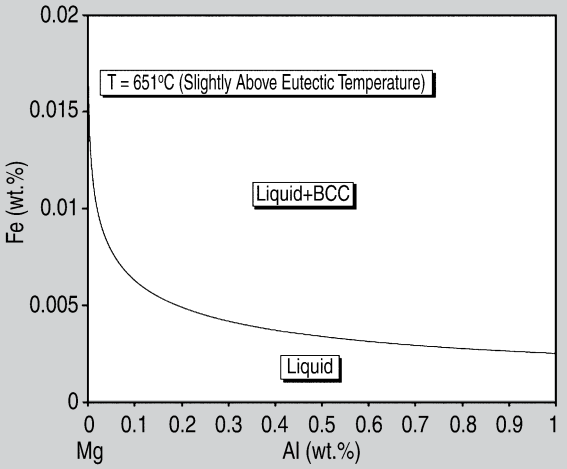

Figure 3. A calculated isothermal section through the Mg-Al-Fe phase diagram.

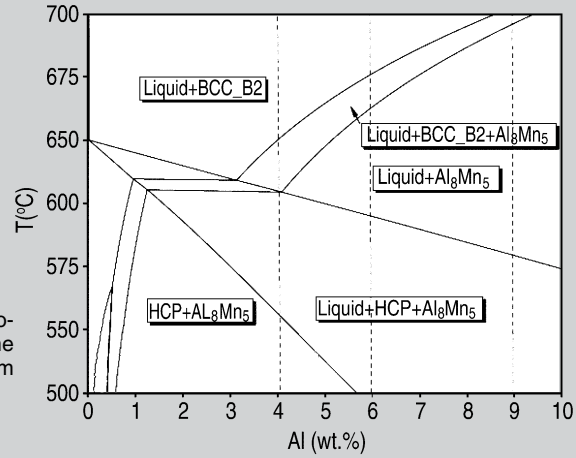

Figure 4. A calculated pseudo-binary section through the Mg-Al-Mn-Fe phase diagram at 0.4%Mn + 0.02%Fe.

Table IV. Summary of the Influence of Composition and Microstructure on the Corrosion of AZ91[7*]

			Salt Spray Corrosion Rate (mm/y)			
Alloy	Mn (%)	Fe/Mn	F	T4	T6	T5
AZ91C	0.18	0.087	18	15	15	—
AZ91E	0.23	0.008	0.64	4	0.15	0.12

*F is as-cast, T4 is solution treated (16 h at 410ºC and quenched), T6 is solution treated and aged (16 h at 410ºC and quenched, 4 h at 215ºC), and T5 is aged (4 h at 215ºC).

$$f_{BCC/casting} = (0.028 - 0.018) / (100 - 0.018) = 0.01\%$$

If this BCC phase is responsible for increasing the corrosion rate by a factor of 100 above that of high-purity magnesium, then the BCC phase needs to evolve hydrogen 10^6 times faster than on α-Mg.

Mg-Al-Fe

Figure 3 presents an isothermal section through the Mg-Al-Fe phase diagram, calculated for 651ºC, slightly above the eutectic temperature. This isothermal section indicates that the eutectic point is shifted to lower iron contents and thus the iron tolerance limit decreases rapidly with increasing aluminum content. The trend of decreasing iron tolerance limit with aluminum alloying has been previously documented (Table I). Figure 3 provides a particular numerical prediction and indicates that there is a significant decrease with a few tens of percent of aluminum.

Mg-Al-Mn-Fe

Figure 4 presents a pseudo-binary section calculated through the Mg-Al-Mn-Fe phase diagram at 0.4%Mn and 0.02%Fe; this section was calculated to try to understand the controlled casting experiments (described in the prior section on high-purity castings) carried out by Hillis and co-workers with AZ91,[6] AM60,[13] and AS4.[10] Figure 4 indicates that cooling of an alloy containing 6% aluminum causes initially the precipitation of an iron-rich BCC phase labeled BCC_B2. Between ~675 and ~670ºC there is a three-phase region of liquid + BCC_B2 + Al_8Mn_5. Following the experiments of Hillis and co-workers[6,10,13] it is assumed that the BCC_B2 phase

settles out as the cast is slowly cooled and that the alloy as-cast at 670ºC contains no BCC_B2 phase but only magnesium liquid + Al_8Mn_5. If it is assumed that the phase Al_8Mn_5 is passive (i.e., it is no more effective as a cathode than pure magnesium) then a 6% aluminum alloy cast at 670ºC has an iron content below the iron tolerance limit and would be expected to show a low corrosion rate.

Thus, Figure 4 predicts the critical temperature at which the alloy is cast to produce a casting with a low corrosion rate to be 670ºC; this calculated critical temperature, T_C, is included in Table II. Similarly, Figure 4 predicts critical temperatures of 690ºC for 9% aluminum (corresponding to AZ91) and 620ºC for 4% aluminum (corresponding to AS41).

Similarly, the pseudo-binary section was calculated through the Mg-Al-Mn-Fe phase diagram at 0.2%Mn + 0.02%Fe and 0.8%Mn + 0.02%Fe to allow comparison with the experiments of Hillis and co-workers starting with 0.2%Mn and 0.8%Mn, respectively. The critical temperatures have been included in Table II, which illustrates a good agreement between the measured critical temperature, T_M, and the calculated critical temperature, T_C, estimated from the calculated phase diagrams. This indicates the phase diagrams are a useful tool for predicting tolerance limits as well as processing parameters.

INFLUENCE OF MICROSTRUCTURE

Table IV provides a summary of the influence of microstructure on the salt spray corrosion performance of AZ91.[7] AZ91C has an iron content greater than the tolerance limit so that the corrosion rate is high and the iron content dominates the behavior; the iron content overwhelms the influence of the microstructure. AZ91E is high purity, the iron content is below the tolerance limit, and there is a clear influence of the microstructure.

The influence of the microstructure has been elucidated in a number of studies,[17] and is well illustrated by the recent study of M.C. Zhao et al.[35] Table V summarizes the corrosion rate measured for 96 h immersion in 1M NaCl solution for high-purity magnesium and high-purity AZ91 in various metallurgical conditions. For as-cast AZ91, the β phase is distributed along the grain boundaries and there is an associated fine lamellar arrangement of α + β so that there is essentially a continuous network. This arrangement of the β phase provides a combination of corrosion barrier effect and micro-galvanic corrosion acceleration. Thus the corrosion rate is significantly greater than that of high-purity magnesium. In the HA3805 and HA3810 conditions, there are large isolated β phase particles so there is significant micro-galvanic corrosion acceleration. In the solution-treated condition (SS), all β is dissolved so that there is a solid solution of ~9% aluminum in the α-Mg matrix. There is no second phase, so the corrosion reflects that of a homogeneous Mg-Al alloy. The aging at 200ºC for the SA205 condition produced fine β precipitates in the α matrix; a more protective surface film is attributed as the cause for the corrosion rate in the SA205 condition to be lower than that of the SS condition.

Table VI illustrates the corrosion rate for AZ80 in different processing conditions, as-cast and extruded.[29] With increasing extrusion temperature more β phase dissolves, leading to a non-continuous β network and thus increased corrosion rate.

Tables V and VI show the same trend in corrosion rate with heat treatment; the corrosion rates produced by solution immersion are considerably higher than those produced by salt spray testing. It is also worth noting that the corrosion rate increased during the immersion tests of Zhao et al.[35] as the corrosion spread across the specimens, indicating that shorter-term tests would measure lower corrosion rates, although the same trends might expect to be measured.

Table V. The Corrosion Rate (mm/y) Measured for 96 h Immersion in 1M NaCl Solution for High-Purity Magnesium and High-Purity AZ91*

As-cast	HA3805	HA3810	SS	SA205	High-Purity Mg
16	24	43	24	6	1

* The following conditions were used: as-cast, HA3805 (homogenization anneal for 5 h at 380ºC plus air cool), HA3810 (homogenization anneal for 10 h at 380ºC plus air cool), SS (100 h at 410ºC plus water quench), and SA205 (SS plus age 5 h at 200ºC).[35]

Table VI. The Corrosion Rate (mm/y) Measured for Immersion in Short Term Tests (~4 h) in 3.5% NaCl Solution for As-cast AZ80 and After Extrusion[29]

As-cast	250ºC	300ºC	350ºC
0.5	7	11	10

RECYCLING AND SECONDARY ALLOYS

The calculated phase diagrams can explain the production of high-purity castings by means of control of melt conditions; this has significance for the production of quality castings from recycled magnesium. As shown by the work of Hillis and co-workers[9–13] using commercial HPDC, high-purity castings can be produced by control of the melt, particularly the melt temperature. The alternative approach is to develop tailored alloys that are less sensitive to the impurity elements (e.g., as by the research of C. Scharf et al).[30]

ACKNOWLEDGEMENTS

This work was supported by the ARC Center of Excellence, Design of Light Alloys. M. Liu and A. Atrens would like to thank EMPA for their support that allowed the authors to spend considerable periods in the EMPA laboratory. EMPA is the Swiss Federal Laboratories for Materials Science and Technology. M. Liu and A. Atrens would also like to thank Ecole Nationale Supérieure de Chimie de Paris (ENSCP) and the Université Pierre et Marie Curie for support that allowed them to spend considerable periods in the Laboratoire de Physico-Chimie des Surfaces, CNRS-ENSCP (UMR 7045), Ecole Nationale Supérieure de Chimie de Paris (ENSCP), 11 rue Pierre et Marie Curie, 75005 Paris, France.

References

1. G. Song and A. Atrens, *Advanced Engineering Materials,* 1 (1999), p. 11.
2. G.L. Song and A. Atrens, *Advanced Engineering Materials,* 5 (2003), p. 837.
3. G. Song and A. Atrens, *Advanced Engineering*

Materials, 9 (2007), pp. 177–183.
4. G.L. Makar and J. Kruger, *International Materials Reviews,* 38 (1993), p. 138.
5. J.D. Hanawalt, C.E. Nelson, and J.A. Peloubet, *Trans. AIME,* 147 (1942), p. 273.
6. K.N. Reichek, K.L. Clark, and J.E. Hillis, *SAE Technical Paper 850417* (Warrendale, PA: SAE, 1985).
7. A. Froats et al., *Metal Handbook, 9th ed., Vol. 13* (Materials Park, OH: ASM International, 1987), pp. 740–754.
8. O. Lunder, T.K. Aune, and K. Nisancioglu, *Corrosion,* 43 (1987), p. 291.
9. J.E. Hillis, *SAE Technical Paper 830523* (Warrendale, PA: SAE, 1983).
10. J.E. Hillis and S.O. Shook, *SAE Technical Paper 890205* (Warrendale, PA: SAE, 1989).
11. J.E. Hillis and R.W. Murray (Presentation at the SDCE 14th International Die Casting Congress and Exposition, Toronto, Canada, 1987), Paper No. G-T87-003.
12. J.E. Hillis and K.N. Reichek, *SAE Technical Paper 860288* (Warrendale, PA: SAE, 1986).
13. W.E. Mercer II and J.E. Hillis, *SAE Technical Paper 920073* (Warrendale, PA: SAE, 1992).
14. O. Lunder et al., *Corrosion,* 45 (1989), p. 741.
15. G. Song, A.L. Bowles, and D.H. StJohn, *Materials Science and Engineering A,* 366 (2004), p. 74.
16. R. Ambat, N.N. Aung, and Z. Zhou, *Corrosion Science,* 42 (2000), p. 1433.
17. G. Song, A. Atrens, and M. Dargusch, *Corrosion Science,* 41 (1998), p. 249.
18. Z. Shi, G. Song, and A. Atrens, *Corrosion Science,* 47 (2005), p. 2760.
19. A. Pardo et al., *Corrosion Science,* 50 (2008), p. 823.
20. A. Prado et al., *Electrochimica Acta,* 53 (2008), p. 7890.
21. M.C. Zhao et al., *Advanced Engineering Materials,* 10 (2008), p. 104.
22. Z. Shi, G. Song, and A. Atrens, *Surface and Coatings Technology,* 201 (2006), p. 492.
23. G. Song and D. StJohn, *Journal of Light Metals,* 2 (2002), p. 1.
24. G. Ballerini et al., *Corrosion Science*, 47 (2005), pp. 2173–2184.
25. Z. Xuehua et al., *Corrosion Science*, 48 (2006), p. 4223.
26. O. Lunder, K. Nisancciogluu, and R.S. Hansen (Presentation at Corrosion of Die Cast Magnesium-Aluminum Alloys, Detroit, MI, February/March 1993).
27. A. Srinivasan et al., *Intermetallics*, 15 (2007), pp. 1511–1517.
28. J. Zhang et al., *Journal of Alloys and Compounds*, (2008), doi:10.1016/j.jallcom.2008.03.089.
29. M.B. Haroush et al., *Corrosion Science,* 50 (2008), p. 1766.
30. C. Scharf et al., *Advanced Engineering Materials,* 7 (2005), p. 1134.
31. C. Hoog, N. Birbilis, and Y. Estrin, *Advanced Engineering Materials,* 10 (2008), p. 579.
32. A. Atrens and W. Dietzel, *Advanced Engineering Materials,* 9 (2007), pp. 292–297.
33. S. Bender, J. Goellner, and A. Atrens, *Advanced Engineering Materials*, 10 (2008), p. 583.
34. M.C. Zhao et al., *Advanced Engineering Materials*, 10 (2008), p. 93.
35. M.C. Zhao et al., *Corrosion Science*, 50 (2008), p. 1939.
36. Ming-Chun Zhao et al., *Corrosion Science,* (2008), doi: 10.1016/j.corsci.2008.08.023.
37. G.L. Song et al., *Corrosion Science,* 39 (1997), pp. 855–875.
38. G.L. Song et al., *Corrosion Science,* 39 (1997), pp. 1981–2004.
39. M. Liu et al., *Scripta Materialia*, 58 (2008), pp. 421–424.
40. J.X. Jia et al., *Materials and Corrosion,* 56 (2005), pp. 468–474.
41. J.X. Jia, G.L. Song, and A. Atrens, *Corrosion Science,* 48 (2006), pp. 2133–2153.
42. J.X. Jia, G. Song, and A. Atrens, *Advanced Engineering Materials,* 9 (2007), pp. 65–74.
43. Y. Wan et al., *Materials & Design*, 29 (2008), pp. 2034–2037.
44. Y. Wang et al., *Materials Letters*, 62 (2008), pp. 2181–2184.
45. M.B. Kannan and R.K. Singh Raman, *Biomaterials*, 29 (2008), pp. 2306–2314.
46. M. Jönsson, D. Persson, and C. Leygraf, *Corrosion Science*, 50 (2008), pp. 1406–1413.
47. T. Zhang et al., *Electrochimica Acta*, 53 (2007), pp. 561–568.
48. G. Ben-Hamu et al., *Materials Science and Engineering: A*, 452-453 (2007), pp. 210–218.
49. G. Song, *Corrosion Science*, 49 (2007), pp. 1696–1701.
50. M. Jönsson, D. Persson, and D. Thierry, *Corrosion Science*, 49 (2007), pp. 1540–1558.
51. J. Chen et al., *Electrochimica Acta*, 52 (2007), pp. 3299–3309.
52. N. Hara et al., *Corrosion Science*, 49 (2007), pp. 166–175.
53. X. Zhou et al., *Corrosion Science*, 48 (2006), pp. 4223–4233.
54. T. Zhang, Y. Li, and F. Wang, *Corrosion Science*, 48 (2006), pp. 1249–1264.
55. M.P. Staiger et al., *Biomaterials,* 27 (2006), pp. 1728–1734.
56. F. Witte et al., *Biomaterials*, 27 (2006), pp. 1013–1018.
57. A.-M. Lafront et al., *Electrochimica Acta*, 51 (2005), pp. 489–501.
58. G. Wu et al., *Journal of Applied Electrochemistry,* 38 (2008), pp. 251–257.
59. J.W. Chang et al., *Journal of Applied Electrochemistry*, 38 (2008), p. 207.
60. A.D. Südholz et al., *Journal of Alloys and Compounds,* (2008), doi:10.1016/j.allcom.2008.03.128.
61. N. Winzer et al., *Advanced Engineering Materials,* 7 (2005), pp. 659–693.
62. N. Winzer et al., *Materials Science and Engineering A*, 472 (2008), p. 97.
63. N. Winzer et al., *Metallurgical and Materials Transactions A,* 39 (2008), p. 1157.
64. M. Bobby Kannan et al., *Materials Science and Engineering A*, 480 (2008), pp. 529–539.
65. N. Winzer et al., *Materials Science and Engineering A*, 488 (2008), p. 339.
66. N. Winzer et al., *Advanced Engineering Materials,* 10 (2008), p. 453.
67. J. Chen et al., *Materials Science and Engineering A*, 488 (2008), pp. 428–434.
68. J. Chen et al., *Electrochemistry Communications*, 10 (2008), pp. 577–581.
69. H. Uchida et al., *Environment-Induced Cracking of Materials,* ed. S. Shipilov et al. (St. Louis, MO: Elsevier, 2008), pp. 323–332.
70. M. Bobby Kannan et al., *Scripta Materialia*, 57 (2007), pp. 579–581.
71. G. Song, A. Atrens, and D.H. StJohn, *Magnesium Technology 2001*, ed. J. Hryn (Warrendale, PA: TMS, 2001), p. 255.
72. *Pandat* software (CompuTherm, Madison, WI), *www.computherm.com/pandat.html.*

Ming Liu and Andrej Atrens are with The University of Queensland, Division of Materials, ARC CoE for Design in Light Metals, Brisbane, Qld 4072, Australia; and also Swiss Federal Laboratories for Materials Science and Technology, Uberlandstrasse 129, CH-8600 Dubendorf, Switzerland. Patrik Schmutz is with Swiss Federal Laboratories for Materials Science and Technology in Dubendorf, Switzerland; and Peter J. Uggowitzer is with ETH Zurich, Department of Materials, CH-8093 Zurich, Switzerland. Prof. Atrens can be reached at andrejs.atrens@uq.edu.au.